Propagation modeling and path loss prediction tools for high frequency surface wave radars

Gökhan APAYDIN[1], **Levent SEVGİ**[2]
[1]*Department of Electrical and Electronics Engineering, Zirve University*
Kızılhisar Kampüs, 27260, Gaziantep-TURKEY
e-mail: gokhanapaydin@zirve.edu.tr
[2]*Department of Electronics and Communication Engineering, Doğuş University*
Zeamet Sokak, No. 21, Acıbadem, 34722, İstanbul-TURKEY
e-mail: lsevgi@dogus.edu.tr

Abstract

Propagation modeling and simulation approaches for the use of High Frequency Surface Wave Radar (HFSWR) are discussed. HFSWR uses vertically polarized surface waves along multi-mixed paths in the lower HF band (3 MHz - 15 MHz). Various numerical propagators are reviewed with an early analytical model. Split Step Fast Fourier Transformation, finite- difference, and finite-element solutions of the well-known one-way, forward propagation Parabolic Equation (PE) model are presented. MATLAB-based numerical propagation prediction tools based on these models are listed. Tests and comparisons among these analytical and numerical tools are given for some canonical surface wave propagation scenarios. The Millington effect for both smooth and irregular terrain paths, which contain land-sea and sea-land transitions, is also discussed.

Key Words: *Groundwaves, Surface waves, High Frequency, High Frequency Surface Wave Radar, Mixed-Path Propagation, Millington Effect, Path Loss, Parabolic Equation, Finite-Difference Method, Finite Element Method, Split-Step PE Method, Impedance Boundary Condition, Hilly Island Effects.*

1. Introduction

High Frequency Surface Wave Radars (HFSWR) use vertically polarized electromagnetic (EM) waves in the lower half of the HF band (3-15 MHz) [1, 2]. They cover wide sea/ocean areas, and are therefore highly attractive for continuous surveillance of oceans, harbors, straights, etc. Understanding the propagation characteristics over the Earth's surface along realistic propagation paths is essential [3-8] for the prediction of HFSWR system performance, and is also important in HFSWR site survey and coverage planning. Groundwave propagation is dominated by Surface Waves (SW) in this frequency range. Groundwaves have three components: direct waves, ground-reflected waves, and surface waves. As long as the transmitter and receiver are close to surface and/or the range is sufficiently long, the direct and ground reflected waves cancel each other and only SW propagates.

The Earth's curvature and local electrical parameters are important in reaching long ranges. The sea surface is a good conductor, but ground conduction is poor at these frequencies. For example, a 5 MHz signal, which reaches 300 km range over the sea, can attain a range of only 40-50 km over ground for the same transmitter and receiver characteristics.

Estimation of typical path losses between HFSWR and a target at various operating frequencies requires a "good" propagation model. The model environment is a spherical Earth with lossy, irregular/rough surface with a variable refractivity above. The exact solution of this complex problem is yet to be solved; there are only approximate analytical and pure numerical techniques that approach the problem in two-dimensions (2D) for relatively simplified propagation paths [3-42]. Early studies date back to the beginning of the last century [9-19]. The International Telecommunication Union (ITU) has prepared special recommendations for this purpose [3]. Surface wave field strength prediction is fully supported by ITU-R Recommendation P-368-7 for both *homogeneous* and *mixed-path* groundwave propagation problems. It gives a set of predicted field strength vs. distance curves for vertically polarized EM waves in the MF and HF bands for variety of ground conductivity σ_g and relative permittivity ε_g values.

Two available analytical SW propagation models, recommended by the ITU, are the ray-optical plus surface wave model of Norton [9] and the surface guided mode model of Wait [13]. The Norton model is efficient in the interference region within the line-of-sight (LOS); but the Wait model is good in the shadow region. One complex problem in SW modeling is the existence of mixed-paths (i.e., land-sea and sea-land transitions) [10]. The Millington curve fitting approach, endorsed and used in ITU recommendations, is used to account for multi-mixed-path propagation scenarios.

Unfortunately, all of these analytical models are valid only for smooth spherical Earth and cannot take terrain irregularities and atmospheric variations into account. There have only been a few attempts in modeling mixed-path transitions with terrain irregularities. Furutsu developed a mathematical model based on the Green's function representation [13], Monteath [6] used the electromagnetic compensation theorem, and Ott [15] formulated his model via the Volterra integral equation technique. Therefore, studies have focused on pure numerical approaches for the last few decades.

Among the others, the PE technique [27-32] is the most attractive groundwave propagator due to its robustness, low memory requirements, and fast implementation. The use of PE for EM wave propagation in a vertically inhomogeneous medium is first described in [30], but the PE became famous in underwater acoustics after the introduction of the Fourier Spit Step (SSPE) technique by Tappert [27]. The SSPE algorithm was then applied to EM wave propagation above the Earth's surface through the atmosphere. Since then, the PE technique has been improved, augmented with many auxiliary tools, and applied to variety of complex propagation problems. Its multi-mixed path propagation prediction capability has been extended by the application of Discrete Mixed Fourier Transform (DMFT) [32] technique. The SSPE technique has been widely used at VHF and above, basically in the microwave region, especially to investigate wave attenuation, ducting, and anti-ducting conditions due to daily, monthly, as well as yearly atmospheric variations. After the introduction of SSPE, Finite-Difference (FD) [33], and Finite-Element (FE) [43-45] based PE implementations have also appeared in the literature. PE-based wave attenuation models due to hilly island transitions along multi-mixed sea/ocean paths at lower HF frequencies has also been implemented recently [46-49].

This tutorial reviews surface wave propagation prediction methods. First, early analytical approaches are summarized in Sec. II. Then, PE based numerical techniques are reviewed in Sec. III. Examples and canonical

tests are given in Sec. IV in relation to HFSWR site survey and coverage planning. Propagation prediction simulations are performed using the Millington package Groundwave Virtual Prediction Tool (GVPT) and three PE-based simulators (SSMIX, FEMIX, and FDMIX), and compared against each other. Finally, challenges and conclusions are outlined in Sec. V.

2. Early analytical models and Millington package

ITU defines SW path loss as [3]

$$L_p = 10 \log_{10}\left(\frac{P_r}{P_t}\right), \quad P_r = \frac{E^2}{Z_0} \times \frac{\lambda^2}{4\pi}, \tag{1}$$

for a given transmitter receiver separation, in terms of transmit and receive powers (P_t and P_r), where E is the vertical field strength for the received power at an arc distance d. For a $P_t = 1$ kW transmitter (i.e. for a short electric dipole with a dipole moment of $M_0 = 5\lambda/2\pi$ Am), the SW path loss is then calculated from

$$L_p = 142.0 + 20 \log\left(f_{MHz}\right) + 20 \log\left(E_{\mu \ V/m}\right). \tag{2}$$

The problem is then reduced to calculating field strength at an arc distance d over the Earth's surface in the presence of irregular terrains, hilly islands, etc. Although the Perfectly Electrical Conductor (PEC) boundary assumption provides, in general, sufficient approximation at VHF and above (i.e. frequencies higher than 30 MHz), the use of impedance (Cauchy-type) boundary condition (BC) at the Earth's surface becomes essential at HF frequencies and below.

2.1. The Millington curve fitting method

It was Millington who first discovered the sharp signal attenuation and strong recovery at the sea-land and land-sea transitions, respectively [10]. He introduced a curve fitting approach, which is also endorsed by the ITU, where the total field along a multi-mixed propagation path is calculated via the interpolation of the direct and reverse electric fields as $E_T = (E_D + E_R)/2$. Here, E_D and E_R are the fields along direct (source-to-receiver) and reverse (receiver-to-source) paths s_k and r_k, respectively. The recursive equations of the Millington Curve Fitting Method [3, 10] are

$$E_D = \sum_{k=1}^{N} E_k(s_k) - \sum_{k=2}^{N} E_k(s_{k-1}), \tag{3}$$

$$s_k = \sum_{n=1}^{k} d_n = d_1 + d_2 + d_3 + \dots + d_k, \tag{4}$$

$$E_R = \sum_{k=1}^{N} E_k(r_k) - \sum_{k=2}^{N} E_{k-1}(r_k), \tag{5}$$

$$r_k = \sum_{n=1}^{k} d_{N-n+1} = d_N + d_{N-1} + d_{N-2} + \dots + d_{N-k}, \tag{6}$$

where $E_j(d_k)$ represents field strength at a range segment d_k over the jth homogeneous medium.

2.2.   Norton surface wave contribution

The Norton formulation [9] extracts a ray-optical asymptotic approximation from a wavenumber spectral integral representation under the standard atmosphere assumption. Since the space wave cancels out at long ranges (and/or transmitter/receiver on or close to the ground), it is sufficient to use Norton's vertical field component only under the flat-Earth assumption (see, for example [26, 38]):

$$
E_{ver} = 2E_0(1 - u^2 + u^4)F(\kappa), \quad E_0 = -ik_0Z_0M_0\frac{e^{ik_0d}}{4\pi d}, \tag{7}
$$

$$
u^2 = \frac{1}{\bar{\varepsilon}_g}, \ \bar{\varepsilon}_g = \varepsilon_g + i\frac{\sigma_g}{\omega\varepsilon_0}, \quad \kappa = -ik_0\frac{d}{2}u^2(1 - u^2) \ , \tag{8}
$$

where E_0 is field strength at the distance d over PEC flat-Earth, $k_0 = 2\pi/\lambda$ is the free-space wavenumber M_0 is the dipole moment, $Z_0 = 120\pi$, σ_g is the conductivity of ground, and $\bar{\varepsilon}_g$ is the relative complex dielectric constant of ground. The surface wave attenuation function is defined as

$$
F(\kappa) = 1 - i\sqrt{\kappa\pi} \ e^{-\kappa} \ \frac{2}{\sqrt{\pi}} \int\limits_{i\sqrt{\kappa}}^{\infty} e^{-t^2}dt. \tag{9}
$$

The finite-conductivity attenuation function $F(\kappa)$ depends on the range, frequency, and electrical parameters of the ground.

2.3.   Wait's surface wave representation

The Wait formulation restructures the spectral integral as a series of normal modes propagating along the Earth's surface. Wait expressed the attenuation function F for the vertical component of electric field [4,14] under flattened-Earth assumption as

$$
E_{ver} = E_0 \ F(x, x'; z), \tag{10}
$$

with the same E_0 given in (7), and the attenuation function

$$
F(x, x'; z) = \left(\frac{\pi z}{2}\right) \sum_{s=1}^{\infty} \frac{e^{i\beta_s z}}{\beta_s - q^2}, \quad q = imn_0\frac{Z_s}{Z_0}, \quad m = \left(\frac{k_0a}{2}\right)^{1/3}. \tag{11}
$$

Here, x and z are the transverse and longitudinal axes, respectively, a is Earth's radius, and n_0 is the refractive index at Earth's surface. The surface impedance Z_s is given as

$$
Z_s = Z_0 \left[\frac{i\omega\varepsilon_0}{\sigma_g + i\omega\varepsilon_g}\right]^{1/2} \left[1 + \frac{i\omega\varepsilon_0}{\sigma_g + i\omega\varepsilon_g}\right]^{1/2}. \tag{12}
$$

For standard atmosphere with inclusion of the Earth's curvature, the transverse mode functions are the solutions of the Airy equation [12],

$$
W(\beta) = \sqrt{\pi} \ [Bi(\beta) - iAi(\beta)] \ , \tag{13}
$$

which satisfy the impedance (Cauchy-type) BC on the Earth's surface

$$\left[\frac{d}{d\beta}W(\beta) - qW(\beta)\right]_{\beta=\beta_s} = 0, \tag{14}$$

and the radiation condition at $x \to \infty$.

The Norton and Wait formulations parameterize the propagation process in terms of different phenomenological models, their ranges of validity, accuracy, rate of convergence, etc., depending on problem parameters, such as operational frequencies, source/observer locations and the physical propagation environment, which differ as well, with particular impact on computations. The WAVEPROB algorithm [24] combines the best features of the Norton and Wait algorithms in an efficient, adaptive format; it uses the Norton formulation at short ranges and then switches to the Wait formulation. A modified version of WAVEPROB has also been introduced as a MATLAB based SW propagation prediction virtual tool GVPT [38]. The GVPT has been widely used to generate field strength predictions, especially for novel broadcast systems. such as Digital Radio Mondiale (DRM). Both WAVEPROB and GVPT deal with smooth-boundary problems, and therefore cannot handle problems such as propagation over irregular/rough surface. Also, propagation prediction through surface and/or elevated ducts formed by inhomogeneous vertical as well as horizontal atmospheric conditions is not possible with these analytical models.

3.   Parabolic wave equation

The standard parabolic wave equation, under $\exp(-i\omega t)$ time dependence, is given as [32]

$$\left\{\frac{\partial^2}{\partial x^2} + 2ik_0\frac{\partial}{\partial z} + k_0^2(n^2 - 1)\right\} u(z,x) = 0, \tag{15}$$

where u denotes the wave amplitude, x and z represent height and range (see Figure 1), respectively, and n is the refractive index. The transverse BC at the surface is $(\alpha_1\partial/\partial x + \alpha_2)\,u(z,x)| = 0$, where α_1 and α_2 are constants for the homogeneous path, and $\alpha_j = 0$ $(j = 1, 2)$ results in Dirichlet and Neumann BCs for the PEC surface, respectively. The impedance BC, for vertical and horizontal polarizations, respectively, are introduced with $\alpha_1 = 1$; $\alpha_2 = ik_0\sqrt{\gamma - 1}/\gamma$ and $\alpha_2 = ik_0\sqrt{\gamma - 1}$ $(\gamma = \varepsilon_g + i60\sigma_g\lambda)$ in terms of surface parameters $(\sigma_g$ and $\varepsilon_g)$. The radiation BC holds for $x \to \infty$ and $z \to \pm\infty$.

The standard fast Fourier transform (FFT) based SSPE solution is:

$$u(z_0 + \Delta z, x) = \exp\left[i\frac{k_0}{2}(n^2 - 1)\Delta z\right] F^{-1}\left\{\exp\left[-i\frac{k_x^2\Delta z}{2k_0}\right] F\left\{u(z_0, x)\right\}\right\}, \tag{16}$$

and can be used to calculate $u(z, x)$ along z with range steps of Δz once the initial field distribution $u(z_0, x)$ is given. The numerical marching solution in (16) represents 2D flat Earth, but Earth's curvature effect is included by adding the term $2x/a_e$ to the refraction index (i.e., $n \to n + 2x/a_e$), where a_e is the Earth's effective radius. Note that the PE in (16) yields waves that are attenuated in 2D, therefore results should be divided by the square root of range in order to obtain path loss vs. range variations in 3D. Although PE in 2D describes one-way propagation and cannot take backscattered waves into account, this is not a serious
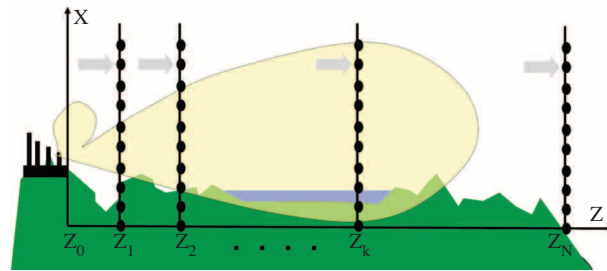
Figure 1. The 2D HFSWR propagation scenario with the transverse x and longitudinal z coordinates. The 2D domain extends from Earth's surface to a maximum height specified by the user-parameters. The surface wave propagation path contains irregular land and smooth sea paths which are both modeled with Cauchy-type (impedance) BCs. A monopole transmit array illuminates the propagation region with a broad beam by exciting vertically polarized EM waves. Typical vertical and horizontal beams of the transmit array are $45°$-$60°$ and $100°$-$120°$, respectively. PE-based one-wave numerical propagators takes a vertical input field profile at a finite number of discrete height points and progress longitudinally step by step. Irregular terrain effects and the Earth's curvature effect are all included in the refractive index of the lower atmosphere.

restriction for propagation engineers who investigate waves emanating from a transmit antenna and reaching a receiver [32].

There is no natural boundary upward in height, therefore waves propagating upwards either go to infinity or are bent down because of the refractivity variations. In either case, the vertical numerical computation space must be terminated at a certain height. The abrupt termination introduces artificial reflections, therefore proper treatment is required above a height of interest and these artificial downward reflections must be eliminated or attenuated to a level much less than the lowest signal.

Irregular terrain modeling can be implemented in the PE via several different mathematical approaches and it is possible for the user to choose the appropriate one for the problem. The *staircase approximation* of the range-dependent terrain profile is the best and easiest in order to handle Dirichlet-type BC, since neither an analytical terrain function nor slope values are required; only the terrain height at each range step is needed. When the terrain height changes, corner diffraction is ignored and the field is simply set to zero on vertical nodes falling on and inside the terrain. Neumann-type BC necessitates the use of *Coordinate Transformation* [32], which is nothing but a simple coordinate transform $z' \rightarrow z$, $x' \rightarrow x - t(z)$, where $t(z)$ is the longitudinal terrain function along the propagation direction. Surface impedance (Cauchy type BC) implementation involves additional modifications; DMFT [32] extends the SSPE algorithm to account for ground losses.

Horizontal and/or vertical refractivity variations (i.e., $n = n(z, x)$), which cause surface and/or elevated duct formations may be implemented in the PE model. It is customary to use refractivity N ($N = (n(z, x) - 1) \times 10^6$) or modified refractivity M ($M = $ N $+$ 157x) with the height x given in kilometers. N is dimensionless, but is measured in "N units" for convenience [5]. For standard atmosphere, the slope of the N and M are "-40N unit/km" and "+117M unit/km", respectively.

The validity range and accuracy limits of the PE-based propagators should be well-understood. First of all, backscattered fields cannot be taken into account in the PE model. Secondly, the results of the PE propagators are not accurate in short regions at high altitudes, since these regions violate the requirement of being inside the paraxial region. Roughly speaking, the range of the observer should be at least five to ten times

greater than the heights of the transmitter and the observer. As an example, for a transmitter located 500 m above the ground, the results of the PE propagators can be accurate at ranges beyond 2.5 km – 5 km, which satisfy a vertical propagation angle of less than $5°$ to $10°$. Note that the vertical coverage may be extended up to $30°$-$40°$ degrees by using wide-angle PE models.

The FFT-based PE solution uses a longitudinally marching procedure. First, an antenna pattern representing the initial height profile is injected. Then, this initial field is propagated longitudinally from z_0 to $z_0 + \Delta z$ via (16) and the transverse field profile at the next range is obtained. This new height profile is then used as the initial profile for the next step and the procedure goes on until the propagator reaches the desired range. SSPE sequentially operates between the vertical domain and the transverse wavenumber domain, which are Fourier transform pairs. SSPE cannot automatically handle the BCs at the Earth's surface. It is satisfied at the surface by removing the surface and taking a mirror copy of the initial vertical field profile below (odd and even symmetric for Dirichlet and Neumann BC, respectively). The physical domain vertically extends to infinity ($x \rightarrow \infty$), therefore an abrupt truncation is required at certain height, which means strong artificial reflections will occur if not taken care of. These non-physical reflections can be removed by using artificial absorbing layers above the height of interest.

The idea of Finite Element (FE) formulation for the PE is to divide the transverse domain between the ground and selected maximum height into sub domains (called elements), use approximated field values at the selected discrete nodes in the vertical domain, and propagate longitudinally by the application of the Crank-Nicholson approach based on the improved Euler method [45]. The initial field at $z = 0$ is generated from a Gaussian antenna pattern specified by its height, vertical beamwidth, and the tilt angle. Note that Crank-Nicholson based longitudinal marching uses Neumann-type BC at each range and Cauchy-type BC is satisfied with the use of (16). Although not necessary, the antenna is located on the surface to better couple surface waves in a short range.

The Finite Difference (FD) formulation of the PE model has also been implemented. The FD-PE is based on the shift-map and finite-difference techniques [33], and allows irregular terrain profiles. Both first- and second-order solutions with respect to the terrain slope effect can be modeled in this approach.

We have developed a MATLAB-based surface wave mixed-path calculator, which we have used in HFSWR coverage planning. It has three main routines: FEMIX, FDMIX, and SSMIX, which use FE, FD, and SSPE approaches, respectively.

4. HFSWR site survey and coverage planning

Propagation prediction tools are extremely important in HFSWR site survey and coverage planning. When HFSWR is of interest, the surveillance area is illuminated on transmit using a broad beam (see Figure 1). Echoes from all objects within the coverage area are received by a linear array of antennas. Beam Synthesis is used to generate simultaneous narrow receive beams. Coherent integration and other signal processing techniques are used to isolate the target signal from the noise and clutter. Return echoes are sorted according to range, velocity (Doppler), and bearing. Returns are compared against a detection threshold chosen to maintain a Constant False Alarm Rate (CFAR). Those returns exceeding the threshold are declared as detections. A Tracking algorithm associates successive detections to form tracks.

A typical HFSWR scenario is pictured in Figure 2. The mission may be to monitor selected traffic

within a selected area, such as coastal regions for off-shore security, waterways or narrow straits for vessel traffic management, etc. Suppose a wide area up to 300 km in range and 120° in azimuth is to be monitored as given in Figure 2. The power budget of the HFSWR is determined from SW path loss calculations. A maximum range of 250-400 km necessitates a low frequency HFSWR and a high power transmitter, since path loss drastically increases with frequency. This is illustrated in Figure 3. Here, path loss vs. range curves over typical sea and land paths at different HF are plotted. As observed, one-way losses may reach up to a few hundred dB for surface wave propagation and this doubles in HFSWRs because of the round trip of the radar signal. For example, the two-way path loss of a 5 MHz signal over sea at 300 km range is nearly 220 dB. This becomes nearly 300 dB at 15 MHz. In other words, the HFSWR signal that reaches 300 km at 5 MHz can only reach up to 60-70 km with the same power at 15 MHz. The average power of typical transmitters is on the order of kWs (between 5 kW – 20 kW) for a HFSWR that operates in the 3 MHz – 6 MHz region.
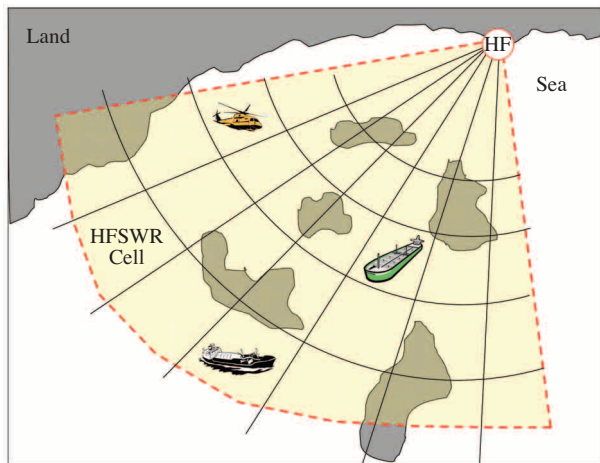
Figure 2. A hypothetic digital map showing a shore based HFSWR location and its coverage. There may be different size islands in the operational area. The aim of this HFSWR is to monitor surface and low-altitude air activities within the operational region.
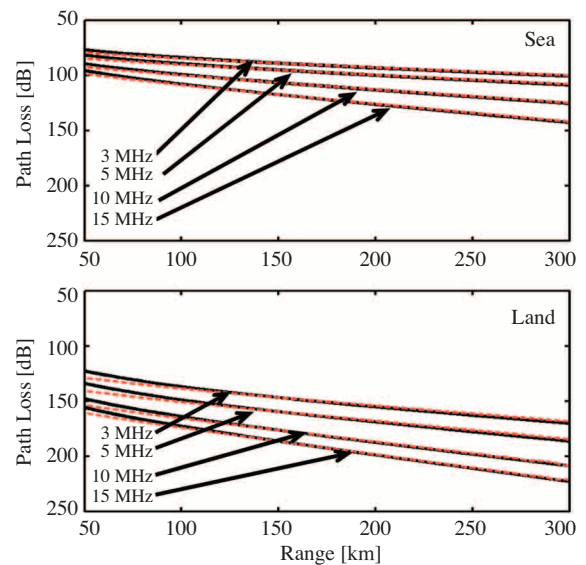

Figure 3. Surface wave sea and land path loss due to a vertically polarized short electric dipole on the surface, with dipole moment $M_0 = 5\lambda/2\pi$ [Am] at various frequencies. Solid curves: Millington GPVT, Dots: SSPE-based propagator. Electrical parameters are: $\sigma = 5$ [S/m], $\varepsilon_r = 80$ for Sea, $\sigma = 0.002$ [S/m], $\varepsilon_r = 10$ for Land.

As shown in Figure 2, there may be many islands along radial sea paths. This necessitates a propagation prediction simulator that can handle multi-mixed paths. Figure 4 presents a typical 2-segment mixed-path propagation simulation. This is the front panel of the MATLAB-based Millington GPVT package [38], which uses Fortran-written executable codes of the Ray-Mode formulations [24]. The effects of the number of multi-mixed paths, path-lengths, electrical parameters of each propagation section, as well as the frequency can easily be investigated with this tool. Here, path loss vs. range curves for various MF and lower HF frequencies for a two-segment propagation path are plotted. The first segment is 50 km over land and the other is 150 km over sea. As observed from the range variation of the path loss, land-sea impedance transition effects cannot be distinguished at 255 kHz and are more effectively distinguishable while increasing the frequency from 1 MHz to 15 MHz.
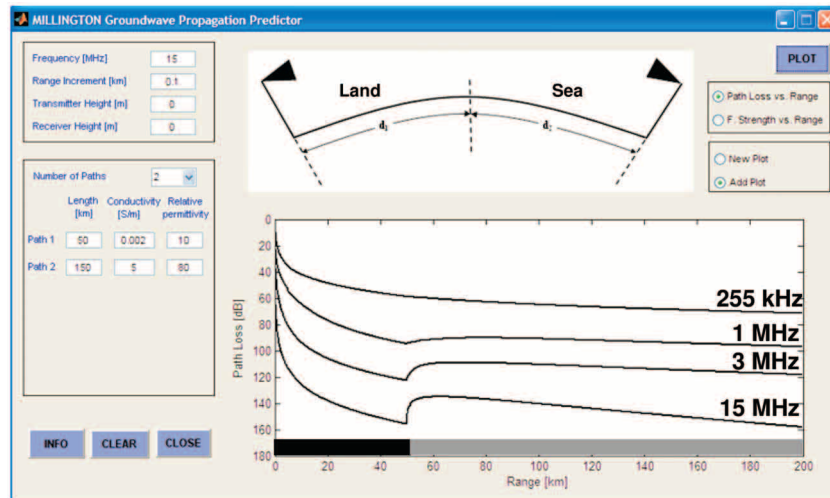
Figure 4. The front panel of the Millington GPVT propagation prediction package and Path loss vs. range curves of various HFSWR frequencies for a 2-segment propagation scenario. The first segment is a 50 km land ($\sigma = 0.002$ [S/m], $\varepsilon_r = 10$) and the other is a 150 km sea path ($\sigma = 5$ [S/m], $\varepsilon_r = 80$).

Figure 5 presents 3D plots of range-height variations of field strengths simulated via PE-based tools (SSPE, FEMPE) [46] with an antenna tilt of 2° at 15 MHz. As observed, the agreement between the results of these tools is impressive. Unfortunately, these 3D plots are mostly good for visualization purposes and are not good for realistic comparisons and calibration. The calibration of such numerical propagators necessitates accurate comparisons. This is achieved via 2D range and/or height illustrations of EM fields as presented in Figure 6. Here, horizontal field variations computed via these tools as field strengths vs. ranges at two different heights, 100 m and 300 m, respectively, are plotted. Very good agreement is clearly observed.
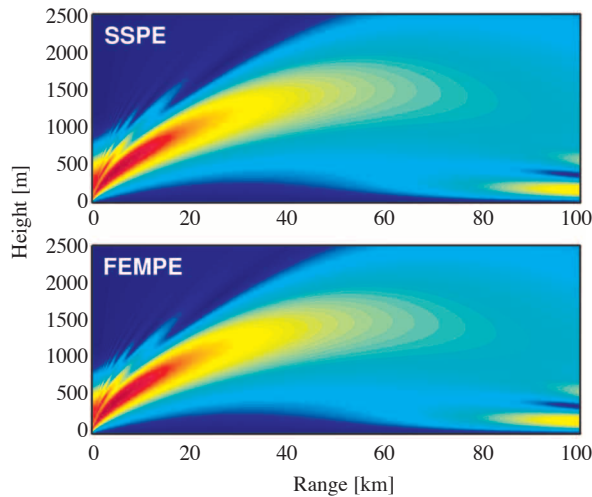

Figure 5. The 3D plots of field strength vs. range-height variations (Top) SSPE, (Bottom) FEMPE results for a given 2° upward tilted Gaussian antenna pattern above PEC ground (f=15 MHz).
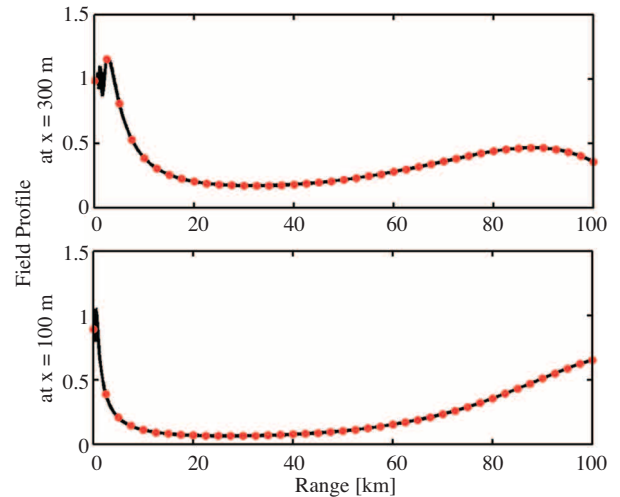

Figure 6. Field strength vs. range at two specified heights; Solid: SSPE, Dotted: FEMPE: (Top) 300 m, (Bottom) 100 m above PEC ground (f=15 MHz).

477

The tests performed above and comparison against the analytical Millington solution may be accepted as a reference to calibrate all SSMIX, FEMIX, and FDMIX propagators for the following figures. It is only after these tests and calibration that one can perform further simulations to predict field strength variation along irregular terrain profiles. Both SSPE and FEMPE can handle propagation problems above irregular terrain profiles through variable atmosphere. The example presented in Figure 7 belongs to the test and comparison over a user specified irregular terrain profile through atmosphere with piecewise bi-linear vertical refractivity variations. Effects of surface BC is presented in Figure 8 at 10 MHz.
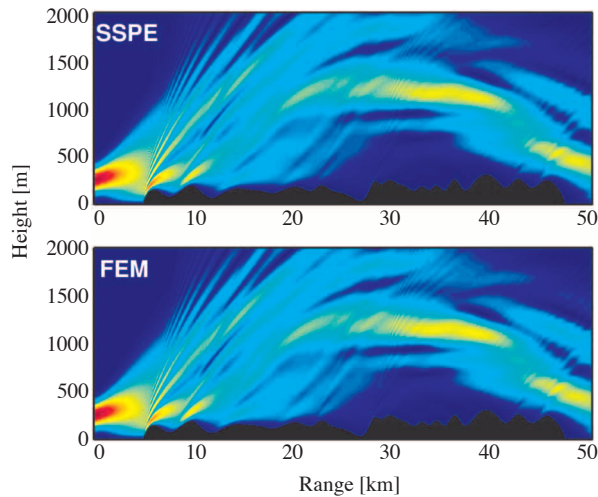

Figure 7. The 3D plots of field strength vs. range-height variations over a user specified non-flat terrain profile (Top) SSPE, (Bottom) FEMPE results (the parameters are taken from Figure 13 in [37] with a frequency of 10 MHz).
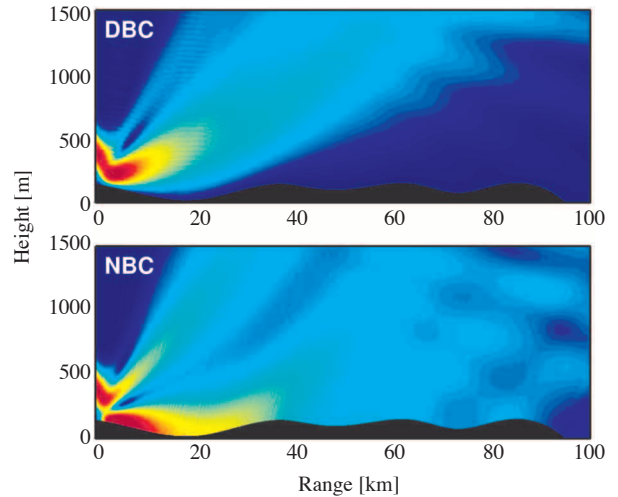
Figure 8. The 3D plots of field strength vs. range-height variations over a user specified non-flat terrain profile with SSPE (Top) Dirichlet BC, (Bottom) Neumann BC (f=10 MHz).

The first path loss predictions along multi-mixed paths are given in Figure 9. In this scenario, there is a 10 km-long island at a distance of 15 km from the transmitter. On top, the signal vs. range/height 3D plot produced with FEMIX at 5 MHz is given. At the bottom, path loss vs. range at different frequencies is plotted and FEMIX is compared against the FDMIX. As observed in these figures, the surface wave detaches from the surface as it propagates because of the Earth's curvature. A small portion follows the surface as the surface wave. When the surface wave reaches the sea-land discontinuity an extra sharp detachment (energy tilt up) occurs. This tilt up explains the sharp attenuation first mentioned by Millington. Signal recovery also occurs at the land-sea discontinuity. Very good agreement between the FDMIX and FEMIX results is clearly observed. The discrepancy at short ranges is because of the artificial location of the surface wave. Further investigations are essential before making speculations on which result is more accurate.

The comparison given in Figure 10 belongs to a 5-segment propagation path. The segment lengths are 15 km–sea, 10 km–land, 5 km–sea, 15 km–land, and 5 km–sea. The curves belong to the predictions at 3 MHz and 15 MHz. Very good agreement between the PE-based SSMIX propagator and GPVT results in all these tests are clearly observed. The discrepancy at ranges close to the transmitter at the lower HF frequencies is because of the surface wave coupling problem in the PE model. This could be overcome by increasing the maximum height and the number of vertical nodes, which increases memory and computation time.
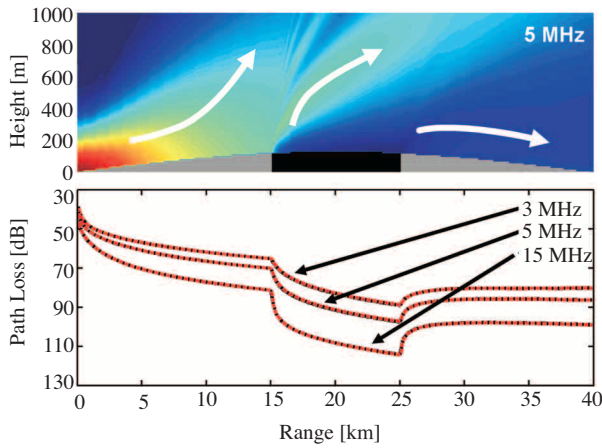
Figure 9. (Top) 3D Signal vs. range/height produced with FEMIX at 5 MHz, (Bottom) Path loss vs. range over a 3-segment 40 km mixed path (a 10 km long island is 15 km away from the transmitter) at 3 MHz, 5 MHz, and 15 MHz (Island: $\sigma = 0.002$ [S/m], $\varepsilon_r = 10$; Sea: $\sigma = 5$ [S/m], $\varepsilon_r = 80$). Solid: FEMIX; Dashed: FDMIX.
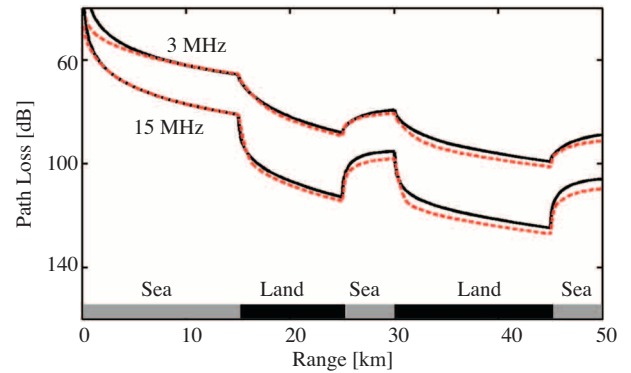
Figure 10. Path loss vs. range over a 5-segment propagation path (10 km and 15 km long islands are 15 km and 30 km away from the source) at 3 MHz and 15 MHz. (Land: $\sigma = 0.002$ [S/m], $\varepsilon_r = 10$; Sea: $\sigma = 5$ [S/m], $\varepsilon_r = 80$). Solid: Millington; Dashed: SSMIX.

Figure 11 belongs to a 30 km long, 3-section path with a Gaussian shaped hilly island. The island is 10 km away from the HFSWR. On top, the 3D Signal vs. range/height plot produced with the PE FDMIX propagator at 5 MHz is given. Wave detachment over the first sea path, energy tilt-up at the sea-land discontinuity, and the tilt up when the wave hits the front slope of the island are clearly observed in the 3D plot. Observe that PE accounts for the attenuation of the SW along the first sea path, the sharp increase in the attenuation at the sea-land discontinuity, signal recovery in the front slope of the island, the additional signal attenuation at the back slope of the island, and finally the signal recovery at the land-sea discontinuity. Path loss vs. range at 5 MHz for this scenario is given at the bottom. The Millington result for the flat island is also shown in the figure. Observe the sharp attenuation at the sea-land discontinuity and signal recovery at land-sea discontinuity, as well as the signal accumulation in the front slope of the island, and additional signal attenuation at the back slope of the island.

Path losses vs. range over the same scenario given in Figure 11 for different island heights at 5 MHz are given in Figure 12. As observed, energy accumulation in the front slope and deep signal loss at the back slope of the island hill increase when the hill height increases.

The effects of the transmitter height and SW coupling onto range variations of signal attenuation are given in Figure 13. Here, a two-hill 25 km-long island is present along a 45 km sea path. The heights of the first and second hills are 250 m and 500 m, respectively. The island is 15 km away from the HFSWR. An elevated antenna is used (a Gaussian shaped antenna pattern with 5° vertical beamwidth is located 500 m above the sea surface). The antenna is tilted 2° downwards. On top, 3D Signal vs. range/height produced at 5 MHz with PE FEMIX propagator is given. At the bottom, path loss vs. range is illustrated with SSMIX and FEMIX propagators at 5 MHz and 15 MHz. Note that the Millington method does not take the island height into account, so the difference between the two curves shows the effects of island height. Observe how surface wave coupling in the near vicinity of the transmitter is important on the signal attenuation and range variations.
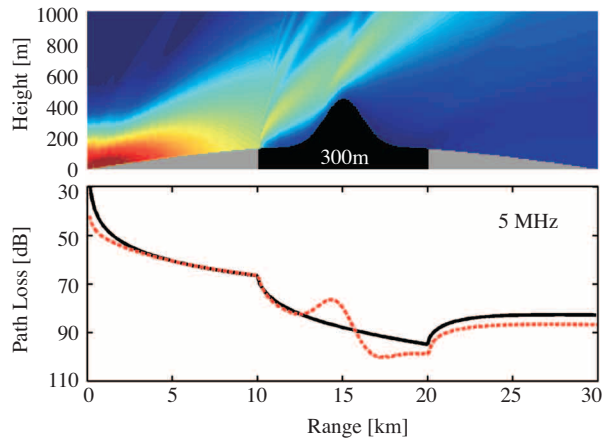
479

Figure 11. The 3D Signal vs. range/height produced with FDMIX at 5 MHz over a 3-segment 30 km mixed path (a 10 km long, 300 m high Gauss-shaped island is 10 km away from the transmitter; Island: $\sigma = 0.002$ [S/m], $\varepsilon_r = 10$; Sea: $\sigma = 5$ [S/m], $\varepsilon_r = 80$).
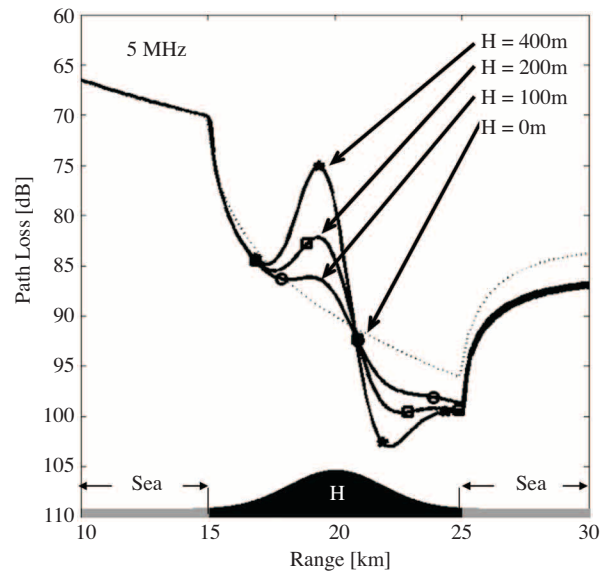
Figure 12. Path loss vs. range over a 3-segment 30 km mixed path (Gauss shaped islands with different heights are 15 km away from the transmitter) at 5 MHz (Island: $\sigma = 0.002$ [S/m], $\varepsilon_r = 10$; Sea: $\sigma = 5$ [S/m], $\varepsilon_r = 80$). Dots: Millington; Others: FEMIX.
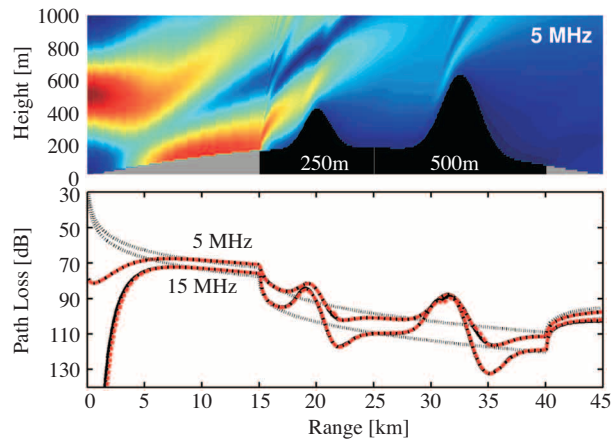

Figure 13. The effects of the transmitter height and surface wave coupling onto range variations of signal attenuation. A Gaussian shaped antenna pattern with $5°$ vertical beamwidth is located 500 m above the sea surface. The antenna is tilted $2°$ downwards: (Top) 3D Signal vs. range/height produced with FEMIX at 5 MHz, (Bottom) Path loss vs. range over a 3-segment 45 km mixed path (a 25 km long, two Gauss-shaped island with 250 m and 500 m maximum height is 15 km away from the transmitter) at 5 MHz and 15 MHz (Island: $\sigma = 0.002$ [S/m], $\varepsilon_r = 10$; Sea: $\sigma = 5$ [S/m], $\varepsilon_r = 80$). Solid: FEMIX; Dashed: SSMIX, Dots: Millington.

The last example belongs to an island with arbitrary terrain profile. In Figure 14, FEMIX and SSMIX PE propagators are compared with each other for a 3-segment 45 km long-mixed-path (with a 25 km long-arbitrary-shaped-island at 10 km) at 3 MHz and 15 MHz.
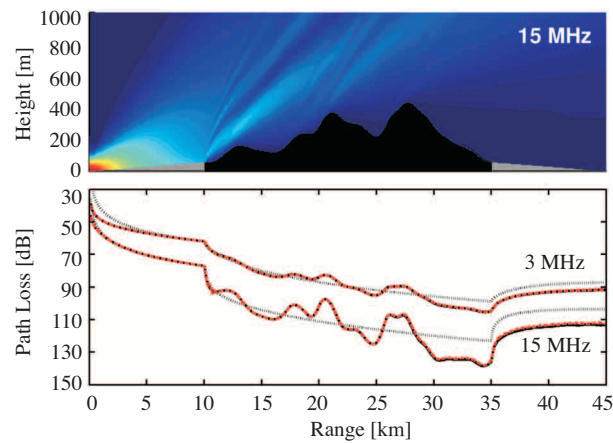
Figure 14. (Top) 3D Signal vs. range/height produced with SSPE at 15 MHz, (Bottom) Path loss vs. range over a 3-segment 45 km mixed path (a 25 km long, arbitrary-shaped island at a distance of 10 km) (Island: $\sigma = 0.002$ [S/m], $\varepsilon_r = 10$; Sea: $\sigma = 5$ [S/m], $\varepsilon_r = 80$). Solid: FEMIX; Dashed: SSMIX, Dots: Millington.

5. Conclusion

Surface wave propagation and path loss predictions for High Frequency Surface Wave Radar site survey and coverage planning is discussed. The problem is to calculate electromagnetic signal attenuation due to 2D wave propagation over spherical Earth paths with impedance boundary conditions on the surface and with multi-mixed paths. Early analytical ray-mode models and the Millington curve fitting approach are reviewed. Propagation prediction tools based on these analytical models, presented before, are summarized. Numerical tools for the Split-step, finite-difference, and finite-element discrete models of the well-known parabolic equation are presented. Tests and comparisons are given along some canonical propagation paths.

References

[1] L. Sevgi, A.M. Ponsford, H.C. Chan. "An integrated maritime surveillance system based on high-frequency surface wave radars, part I – theoretical background and numerical simulations." *IEEE Antennas and Propagation Magazine*, Vol. 43, No. 4, pp. 28-43, Aug. 2001.

[2] A.M. Ponsford, L. Sevgi, H.C. Chan. "An integrated maritime surveillance system based on high-frequency surface wave radars, part II – operational status and system performance." *IEEE Antennas and Propagation Magazine*, Vol. 43, No. 5, pp. 52-63, Oct. 2001.

[3] ITU-R, Recommendations, P-368-7, "Groundwave propagation curves for frequencies between 10 kHz and 30 MHz", International Telecommunications Union, Mar. 1992.

[4] J.R. Wait. *Electromagnetic Waves in Stratified Media.* Oxford: Pergamon Press, 1962.

[5] V.A. Fock. *Electromagnetic Diffraction and Propagation Problems.* Oxford: Pergamon Press, 1965.

[6] G.D. Monteath. *Applications of EM Reciprocity Principle.* Tarrytown, New York: Academic Press, 1973.

[7] L. Sevgi. *Complex Electromagnetic Problems and Numerical Simulation Approaches.* New York: IEEE and John Wiley Press, Jun. 2003.

[8] N.M. Maslin. *HF Communications: A Systems Approach.* London: Pitmann Publishing, 1987 (also in, Taylor & Francis E-Library, 2005).

[9] K.A. Norton. "The propagation of radio waves over the surface of earth and in the upper atmosphere." *in Proc. of the IRE*, Vol. 24, No. 10, pp. 1367-1387, Oct. 1936.

[10] G. Millington. "Groundwave propagation over an inhomogeneous smooth earth." *in Proc. of the IEE (UK)*, Part III, Vol. 96, No. 39, pp. 53-64, Mar. 1949.

[11] H. Bremmer. "The extension of Sommerfeld formula for the propagation of radio waves over a flat-earth, to different conductivities of the soil." *Physica*, Vol. 20, pp. 441-460, 1954.

[12] K. Furutsu. "On the excitation of the waves of proper solutions." *IEEE Trans. Antennas and Propagation*, Vol. 7, No. 5, pp. 209-218, Dec. 1959.

[13] K. Furutsu. "A systematic theory of wave propagation over irregular terrain." *Radio Science*, Vol. 17, No. 5, pp. 1037-1050, 1982.

[14] J.R. Wait, L.C. Walters. "Curves for ground wave propagation over mixed land and sea paths." *IEEE Trans. Antennas and Propagation*, Vol. 11, No. 1, pp. 38-45, Jan. 1963.

[15] R.H. Ott. "A new method for predicting HF ground wave attenuation over inhomogeneous, irregular terrain." *OT/ITS Research Report 7*, Office of Telecommunications/Institute for Telecommunication Sciences, Boulder, Colorado, 1971.

[16] R.H. Ott. "An alternative integral equation for propagation over irregular terrain, II." *Radio Science*, Vol. 6, No. 4, pp. 429-435, 1971.

[17] R.H. Ott, L.E. Vogler, G.A. Hufford. "Ground-wave propagation over irregular inhomogeneous terrain: Comparisons of calculations and measurements." *IEEE Trans. Antennas and Propagation*, Vol. 27, No. 2, pp. 284-286, Feb. 1979.

[18] D.A. Hill, J.R. Wait. "HF ground wave propagation over mixed land, sea, sea-ice paths." *IEEE Trans. Geoscience and Remote Sensing*, Vol. 19, pp. 210-216, 1981.

[19] D.A. Hill, J.R. Wait. "Ground wave propagation over a mixed path with an elevation change." *IEEE Trans. Antennas and Propagation*, Vol. 30, No.1, pp. 139-141, Jan. 1982.

[20] S. Ayasli. "SEKE: A computer model for low altitude radar propagation over irregular terrain." *IEEE Trans. Antennas and Propagation*, Vol. 34, No. 8, pp.1013-1023, Aug. 1986.

[21] L.B. Felsen, L. Sevgi. "Adiabatic and intrinsic modes for wave propagation in guiding environments with longitudinal and transverse variation: formulation and canonical test." *IEEE Trans. Antennas and Propagation*, Vol. 39, No.8, pp. 1130-1136, Aug. 1991.

[22] L.B. Felsen, L. Sevgi. "Adiabatic and intrinsic modes for wave propagation in guiding environments with longitudinal and transverse variations: continuously refracting media." *IEEE Trans. Antennas and Propagation*, Vol. 39 No. 8, pp.1137-1143, Aug. 1991.

[23] J.R. Wait. "The ancient and modern history of EM groundwave propagation." *IEEE Antennas and Propagation Magazine*, Vol. 40, No. 5, pp. 7-24, Oct. 1998.

[24] L. Sevgi, L.B. Felsen. "A new algorithm for ground wave propagation based on a hybrid ray-mode approach." *Int. J. of Numerical Modeling*, Vol. 11, No. 2, pp. 87-103, Mar. 1998.

[25] S.W. Marcus. "A hybrid (finite difference-surface Green's function) method for computing transmission losses in an inhomogeneous atmosphere over irregular terrain." *IEEE Trans. Antennas and Propagation*, Vol. 40, No. 12, pp. 1451-1458, Dec. 1992.

[26] L. Sevgi, F. Akleman, L.B. Felsen. "Ground wave propagation modeling: problem-matched analytical formulations and direct numerical techniques." *IEEE Antennas and Propagation Magazine*, Vol. 44, No. 1, pp. 55-75, Feb. 2002.

[27] F.D. Tappert. "The parabolic approximation method." in *Wave Propagation and Underwater Acoustics*, pp. 224-287 Eds. Keller J.B. and Papadakis, J.S., New York: Springer-Verlag, 1977.

[28] A.E. Barrios. "Parabolic equation modeling in horizontally inhomogeneous environments." *IEEE Trans. Antennas and Propagation*, Vol. 40, No. 7, pp. 791-797, July 1992.

[29] A.E. Barrios. "A terrain parabolic equation model for propagation in the troposphere." *IEEE Trans. Antennas and Propagation*, Vol. 42, No. 1, pp. 90-98, Jan. 1994.

[30] K.H. Craig. "Propagation modeling in the troposphere: parabolic equation method." *IEE Electronics Letters*, Vol. 24, No. 18, pp. 1136-1139, Sep. 1988.

[31] D.J. Donohue, J.R. Kuttler. "Propagation modeling over terrain using the parabolic wave equation." *IEEE Trans. Antennas and Propagation*, Vol. 48, No. 2, pp. 260-277, Feb. 2000.

[32] M. Levy. *Parabolic Equation Methods for Electromagnetic Wave Propagation.* United Kingdom: IEE, Institution of Electrical Engineers, 2000.

[33] P.D. Holm. "Wide-angle shift-map PE for a piecewise linear terrain-a finite-difference approach." *IEEE Trans. Antennas and Propagation*, Vol. 55, No. 10, pp. 2773-2789, Oct. 2007.

[34] F. Akleman, L. Sevgi. "A novel finite difference time domain wave propagator." *IEEE Trans. Antennas and Propagation*, Vol. 48, No. 5, pp. 839-841, May 2000.

[35] F. Akleman, L. Sevgi. "Realistic surface modeling in a time-domain wave propagator." *IEEE Trans. Antennas and Propagation*, Vol. 51, No. 7, pp. 1675-1679, July 2003.

[36] M.O. Ozyalcin, F. Akleman, L. Sevgi. "A novel TLM based time domain wave propagator." *IEEE Trans. Antennas and Propagation*, Vol. 51, No. 7, pp. 1680-1683, July 2003.

[37] L. Sevgi, C. Uluisik, F. Akleman. "A matlab-based two-dimensional parabolic equation radiowave propagation package." *IEEE Antennas and Propagation Magazine*, Vol. 47, No. 4, pp. 164-175, Aug. 2005.

[38] L. Sevgi. "A mixed-path groundwave field strength prediction virtual tool for digital radio broadcast systems in medium and short wave bands." *IEEE Antennas and Propagation Magazine*, Vol. 48, No. 4, pp. 19-27, Aug. 2006.

[39] C.A. Tunc, F. Akleman, V.B. Erturk, A. Altintas, L. Sevgi. "Fast integral equation solutions: Application to mixed path terrain profiles and comparisons with parabolic equation method." *Complex Computing Networks*, Springer in Physics Series, Vol. 104, pp. 55-63, Jan. 2006.

[40] L. Sevgi. "Groundwave modeling and simulation strategies and path loss prediction virtual tools." *IEEE Trans. Antennas and Propagation*, Special issue on Electromagnetic Wave Propagation in Complex Environments: A Tribute to L.B. Felsen,Vol. 55, No. 6, pp. 1591-1598, Jun. 2007.

[41] F. Akleman, L. Sevgi. "A novel MoM- and SSPE-based groundwave propagation field strength prediction simulator." *IEEE Antennas and Propagation Magazine*, Vol. 49, No. 5, pp. 69-82, Oct. 2007.

[42] L. Sevgi. "A numerical Millington propagation package for medium and short wave DRM systems field strength predictions." *IEEE Broadcast Technology Society Newsletter*, Vol. 14, No. 3, pp. 9-11, Fall 2006.

[43] D. Huang. "Finite element solution to the parabolic wave equation." *J. Acoust. Soc. Am.*, Vol. 84, No. 4, pp. 1405-1413, Oct. 1988.

[44] J.-M. Jin. The Finite Element Method in Electromagnetics. New York: John Wiley Press, 2002.

[45] K. Arshad, F.A. Katsriku, A. Lasebae. "An investigation of tropospheric wave propagation over irregular terrain and urban streets using finite elements." *in Proc. 6th WSEAS Conference on Telecommunications and Informatics*, 22-24th March 2007, Dallas TX, USA, pp. 105-110.

[46] G. Apaydin, L. Sevgi. "The split step Fourier and finite element based parabolic equation propagation prediction tools: canonical tests, systematic comparisons, and calibration." *IEEE Antennas and Propagation Magazine*, Vol. 52, No. 3, Jun. 2010.

[47] G. Apaydin, L. Sevgi. "FEM-based surface wave multi-mixed-path propagator and path loss predictions." *IEEE Antennas and Wireless Propagation Letters*, Vol. 8, pp. 1010-1013, 2009.

[48] G. Apaydin, L. Sevgi. "Numerical investigations of and path loss predictions for surface wave propagation over sea paths including hilly island transitions." *IEEE Trans. Antennas and Propagation*, Vol. 58, No. 4, pp. 1302-1314, Apr. 2010.

[49] G. Apaydin, L. Sevgi. "A novel split-step parabolic equation package for surface wave propagation prediction along multi-mixed irregular terrain paths." *IEEE Antennas and Propagation Magazine*, Vol. 52, No. 4, Aug. 2010.